ELectronics EXpress

LETTER

IEICE Electronics Express, Vol.11, No.16, 1–12

A Multi-Scaling Forward-Backward Time-Stepping Method for microwave imaging

Toshifumi Moriyama[1a)], **Giacomo Oliveri**[2b)], **Marco Salucci**[2], **and Takashi Takenaka**[1]

[1] *Department of Electrical and Electronic Engineering, Nagasaki University, Nagasaki 852–8521, Japan*

[2] *ELEDIA Research Center at DISI, University of Trento, Via Sommarive 9, 38123 Trento, Italy*

a) *t-moriya@nagasaki-u.ac.jp*

b) *giacomo.oliveri@unitn.it*

Abstract: This paper is aimed at presenting a new time-domain imaging technique that combines the regularization properties of the Filtered *FBTS* method with an efficient information-acquisition strategy, namely the Iterative Multi-Scaling Approach (*IMSA*). The proposed time-domain approach is then validated by means of a set of preliminary numerical test cases aimed at pointing out its features and potentialities, as well.

Keywords: electromagnetic inverse scattering, Forward-Backward Time Stepping (*FBTS*) Method, Iterative Multi-Scaling Approach (*IMSA*)

Classification: Electromagnetic theory

References

[1] G. C. Giakos, M. Pastorino, F. Russo, S. Chiwdhury, N. Shah and W. Davros: IEEE Instrum. Meas. Mag. **2** (1999) 32. DOI:10.1109/5289.765967

[2] S. Kharkovsky and R. Zoughi: IEEE Instrum. Meas. Mag. **10** (2007) 26. DOI:10.1109/MIM.2007.364985

[3] R. Zoughi: *Microwave Nondestructive Testing and Evaluation* (Kluwer Academic, Amsterdam, The Netherlands, 2000).

[4] P. M. Meaney, M. W. Fanning, D. Li, S. P. Poplack and K. D. Paulsen: IEEE Trans. Microw. Theory Tech. **48** (2000) 1841. DOI:10.1109/22.883861

[5] S. C. Hagness, E. C. Fear and A. Massa: IEEE Antennas Wirel. Propag. Lett. **11** (2012) 1592. DOI:10.1109/LAWP.2013.2240569

[6] M. El-Shenawee and E. Miller: IEEE Trans. Med. Imaging **25** (2006) 1258. DOI:10.1109/TMI.2006.881377

[7] T. Rubk, P. M. Meaney, P. Meincke and K. D. Paulsen: IEEE Trans. Antenn. Propag. **55** (2007) 2320. DOI:10.1109/TAP.2007.901993

[8] J. E. Johnson, T. Takenaka and T. Tanaka: IEEE Trans. Biomed. Eng. **55** (2008) 1941. DOI:10.1109/TBME.2007.899364

[9] H. Zhou, T. Takenaka, J. Johnson and T. Tanaka: PIER **93** (2009) 57. DOI:10.2528/PIER09033001

DOI: 10.1587/elex.11.20140578
Received June 16, 2014
Accepted July 14, 2014
Publicized August 1, 2014
Copyedited August 25, 2014

[10] P. Mojabi and J. LoVetri: IEEE Antennas Wirel. Propag. Lett. **8** (2009) 645. DOI:10.1109/LAWP.2009.2023602
[11] Q. Fang, P. Meaney and K. Paulsen: IEEE Trans. Antenn. Propag. **58** (2010) 449. DOI:10.1109/TAP.2009.2037691
[12] D. Lesselier and T. Habashy, eds.: Inverse Problems **16** (2000).
[13] O. M. Bucci and G. Franceschetti: IEEE Trans. Antenn. Propag. **37** (1989) 918. DOI:10.1109/8.29386
[14] H. Harada, D. J. N. Wall, T. Takenaka and T. Tanaka: IEEE Trans. Antenn. Propag. **43** (1995) 784. DOI:10.1109/8.402197
[15] O. Dorn and D. Lesselier: Inverse Probl. **22** (2006) R67. DOI:10.1088/0266-5611/22/4/R01
[16] M. R. Hajihashemi and M. El-Shenawee: IEEE Antennas Wirel. Propag. Lett. **7** (2008) 92. DOI:10.1109/LAWP.2008.920464
[17] R. Aramini, G. Caviglia, A. Massa and M. Piana: Inverse Probl. **26** (2010) 055004. DOI:10.1088/0266-5611/26/5/055004
[18] G. Oliveri, A. Randazzo, M. Pastorino and A. Massa: J. Opt. Soc. Am. A **29** (2012) 945. DOI:10.1364/JOSAA.29.000945
[19] M. Salucci, G. Oliveri, A. Randazzo, M. Pastorino and A. Massa: J. Opt. Soc. Am. A **31** (2014) 1167. DOI:10.1364/JOSAA.31.001167
[20] M. D'Urso, T. Isernia and A. Morabito: IEEE Trans. Geosci. Rem. Sens. **48** (2010) 1186. DOI:10.1109/TGRS.2009.2032175
[21] P. Mojabi and J. LoVetri: IEEE Trans. Antenn. Propag. **57** (2009) 2658. DOI:10.1109/TAP.2009.2027161
[22] P. Mojabi and J. LoVetri: IEEE Trans. Antenn. Propag. **59** (2011) 1597. DOI:10.1109/TAP.2011.2123066
[23] G. Oliveri, P. Rocca and A. Massa: IEEE Trans. Geosci. Rem. Sens. **49** (2011) 3993. DOI:10.1109/TGRS.2011.2128329
[24] G. Oliveri, L. Poli, P. Rocca and A. Massa: Opt. Lett. **37** (2012) 1760. DOI:10.1364/OL.37.001760
[25] L. Poli, G. Oliveri and A. Massa: IEEE Trans. Antenn. Propag. **60** (2012) 2865. DOI:10.1109/TAP.2012.2194676
[26] L. Poli, G. Oliveri, P. Rocca and A. Massa: IEEE Trans. Geosci. Rem. Sens. **51** (2013) 2920. DOI:10.1109/TGRS.2012.2218613
[27] L. Poli, G. Oliveri, F. Viani and A. Massa: IEEE Trans. Antenn. Propag. **61** (2013) 4722. DOI:10.1109/TAP.2013.2265254
[28] F. Viani, L. Poli, G. Oliveri, F. Robol and A. Massa: Microw. Opt. Technol. Lett. **55** (2013) 1553. DOI:10.1002/mop.27612
[29] L. Poli, G. Oliveri and A. Massa: J. Opt. Soc. Am. A **30** (2013) 1261. DOI:10.1364/JOSAA.30.001261
[30] C. Gilmore, P. Mojabi, A. Zakaria, M. Ostadrahimi, C. Kaye, S. Noghanian, L. Shafai, S. Pistorius and J. LoVetri: IEEE Trans. Biomed. Eng. **57** (2010) 894. DOI:10.1109/TBME.2009.2036372
[31] C. Eyraud, J. M. Geffrin and A. Litman: IEEE Trans. Antenn. Propag. **59** (2011) 1237. DOI:10.1109/TAP.2011.2109353
[32] T. Takenaka, T. Tanaka, H. Harada and S. He: Microw. Opt. Technol. Lett. **16** (1997) 292. DOI:10.1002/(SICI)1098-2760(19971205)16:5<292::AID-MOP8>3.0.CO;2-A
[33] T. Tanaka, T. Takenaka and S. He: Microw. Opt. Technol. Lett. **20** (1999) 72. DOI:10.1002/(SICI)1098-2760(19990105)20:1<72::AID-MOP19>3.0.CO;2-4
[34] T. Tanaka, N. Kuroki and T. Takenaka: J. Electromagn. Waves Appl. **17** (2003) 253. DOI:10.1163/156939303322235815
[35] P. Rocca, M. Benedetti, M. Donelli, D. Franceschini and A. Massa: Inv. Probl. **25** (2009) 1. DOI:10.1088/0266-5611/25/12/123003
[36] S. Caorsi, A. Massa and M. Pastorino: IEEE Trans. Geosci. Rem. Sens. **38**

DOI: 10.1587/elex.11.20140578
Received June 16, 2014
Accepted July 14, 2014
Publicized August 1, 2014
Copyedited August 25, 2014

(2000) 1697. DOI:10.1109/36.851968
[37] A. Breard, G. Perrusson and D. Lesselier: IEEE Geosci. Remote Sens. Lett. **5** (2008) 788. DOI:10.1109/LGRS.2008.2005790
[38] P. Rocca, G. Oliveri and A. Massa: IEEE Antennas Propag. Mag. **53** (2011) 38. DOI:10.1109/MAP.2011.5773566
[39] S. Caorsi, M. Donelli, D. Franceschini and A. Massa: IEEE Trans. Microw. Theory Tech. **51** (2003) 1162. DOI:10.1109/TMTT.2003.809677
[40] G. Franceschini, D. Franceschini and A. Massa: IEEE Geosci. Remote Sens. Lett. **2** (2005) 428. DOI:10.1109/LGRS.2005.853200
[41] A. Baussard, E. L. Miller and D. Lesselier: Inverse Probl. **20** (2004) S1. DOI:10.1088/0266-5611/20/6/S01
[42] M. Benedetti, D. Lesselier, M. Lambert and A. Massa: IEEE Trans. Geosci. Rem. Sens. **48** (2010) 2330. DOI:10.1109/TGRS.2009.2039144
[43] G. Oliveri, Y. Zhong, X. Chen and A. Massa: J. Opt. Soc. Am. A **28** (2011) 2057. DOI:10.1364/JOSAA.28.002057
[44] G. Oliveri, L. Lizzi, M. Pastorino and A. Massa: IEEE Trans. Antenn. Propag. **60** (2012) 971. DOI:10.1109/TAP.2011.2173131
[45] T. Isernia, V. Pascazio and R. Pierri: IEEE Trans. Geosci. Rem. Sens. **39** (2001) 1596. DOI:10.1109/36.934091

1 Introduction

The development of reliable procedures for the solution of electromagnetic inverse scattering problems has received a growing attention in the last years due to their occurrence in *NDE*/*NDT* [1, 2, 3], biomedical diagnostics [4, 5, 6, 7, 8, 9, 10, 11], and geophysical applications [12]. Nevertheless, general-purpose and efficient inversion methodologies are often not available because of the intrinsic drawbacks of the problems at hand, namely the ill-posedness and strong non-linearity [13].

By reviewing the state-of-the-art literature, several techniques have been successfully developed in the frequency domain under the assumption of monochromatic illuminations [14, 15, 16, 17, 18, 19, 20, 21, 22, 23, 24, 25, 26, 27, 28, 29]. Despite their success, such inversion methods often present some limitations since only a reduced amount of information is actually retrievable from a single frequency measurement [30] and the exploitation of higher frequencies to enhance the spatial resolution [30, 31] generally causes an increase of the complexity of the measurement system [31]. In order to overcome these limitations, the use of broadband measurement systems has been proposed [9, 30, 31, 32, 33, 34]. In such a framework, time-domain inversions are often preferred because of the enhanced efficiency and reliability especially when wide bandwidths are at hand [9, 32, 33, 34]. However, the development of suitable approaches is not trivial since (*a*) ill-posedness and (*b*) non-linearity still hold true [32, 33, 34]. With reference to the ill-posedness, *regularization* techniques based on data-filtering have been introduced to mitigate the numerical instabilities of the retrieved solutions [34]. For instance, the combination of an iterative low-pass filtering approach with the Forward-Backward Time-Stepping (*FBTS*) allows one to yield good results when dealing with noisy data [34].

DOI: 10.1587/elex.11.20140578
Received June 16, 2014
Accepted July 14, 2014
Publicized August 1, 2014
Copyedited August 25, 2014

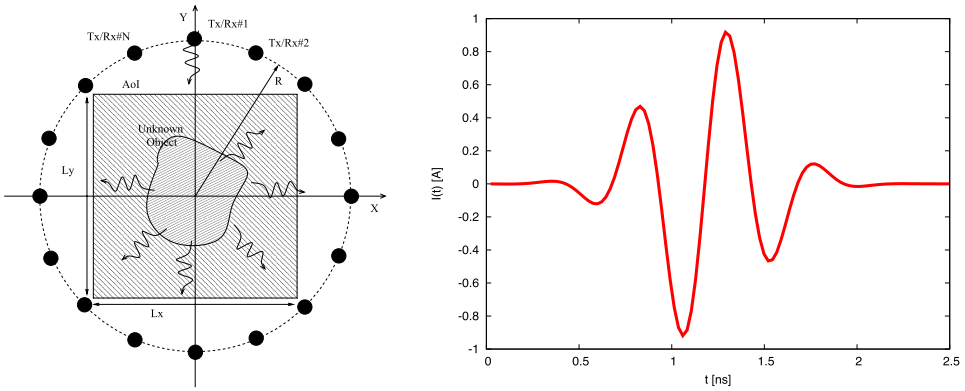

(a) (b)

Fig. 1. Problem geometry (*a*) and illumination time-pulse (*b*).

On the other hand, global optimization tools, already and successfully applied in the frequency domain [35, 36, 37, 38], are still viable solutions to counteract the *local minima* issues associated to nonlinearity. However, *information-acquisition* strategies based on multi-resolution expansions [39, 40, 41, 42, 43, 44] seem to be a more suitable choice for time-domain approaches. Indeed, the computational efficiency of the algorithmic tools is a key requirement when dealing with broadband scattered data because of the intrinsically cumbersome numerical burden of time-domain inversions [9, 34].

This paper is then aimed at presenting an innovative time-domain microwave imaging approach that integrates the Filtered *FBTS* method into an efficient multi-resolution technique, namely the Iterative Multi-Scaling Approach (*IMSA*), to effectively address both the ill-posedness/ill-conditioning and the non-linearity of time-domain electromagnetic inversion problems.

2 Problem formulation

Let us consider a two-dimensional investigation domain Ω that contains an unknown scatterer [Fig. 1(*a*)]. The object is embedded in a homogeneous background with permittivity ε_0 and permeability μ_0 and it is successively illuminated by V short-pulsed waves generated by line current sources parallel to the z axis [33]

$$J_z^{(v)}(\underline{r},t) = I(t)\delta\big(\underline{r}-\underline{r}^{(v)}\big), \quad v=1,\ldots,V \tag{1}$$

where $\underline{r}=(x,y)$ is the position vector, $\underline{r}^{(v)}$ indicates the v-th transmitter location, $I(t)$ is the "pulse shape", and $\delta(\underline{r})$ is the Dirac delta function. Under these assumptions, the total electric and magnetic fields in correspondence with the v-th excitation obey Maxwell's equations as indicated in the following compact time-domain form [34]

$$\begin{cases} \mathcal{L}\underline{f}^{(v)}(\underline{r},t) = \underline{J}^{(v)}(\underline{r},t) \\ \underline{f}^{(v)}(\underline{r},t=0) = \underline{0} \end{cases} \quad \underline{r}\in\Omega,\ t\in[0,T] \tag{2}$$

DOI: 10.1587/elex.11.20140578
Received June 16, 2014
Accepted July 14, 2014
Publicized August 1, 2014
Copyedited August 25, 2014

where T is the time horizon, $\underline{f}^{(v)}(\underline{r},t) \triangleq \left(E_z^{(v)}(\underline{r},t), \eta H_x^{(v)}(\underline{r},t), \eta H_y^{(v)}(\underline{r},t)\right)'$ ($'$ being the transpose operator), $\underline{J}^{(v)}(\underline{r},t) \triangleq \left(0,0,J_z^{(v)}(\underline{r},t)\right)'$, and $\eta \triangleq \sqrt{\frac{\mu_0}{\varepsilon_0}}$ is the background impedance. It is worth noticing that the second equation in (2) enforces the initial condition (i.e., null field at $t=0$). Moreover, the explicit form of the differential operator $\mathcal{L}$ is given by [34]

$$\mathcal{L} = \mathbf{A}\frac{\partial}{\partial x} - \mathbf{B}\frac{\partial}{\partial y} - \mathbf{C}\frac{\partial}{\partial (ct)} - \mathbf{D} \tag{3}$$

where $c \triangleq 1/\sqrt{\mu_0\varepsilon_0}$, $\mathbf{A} \triangleq \{A_{ij},\ i=1,\ldots,3,\ j=1,\ldots,3; A_{31}=A_{13}=1, A_{ij}=0\ otherwise\}$, $\mathbf{B} \triangleq \{B_{ij},\ i=1,\ldots,3,\ j=1,\ldots,3; B_{21}=B_{12}=1, B_{ij}=0\ otherwise\}$, $\mathbf{C} \triangleq diag(\varepsilon(\underline{r}),\mu(\underline{r}),\mu(\underline{r}))'$, $\mathbf{D} \triangleq diag(\eta\sigma(\underline{r}),1,1)$, and $\varepsilon(\underline{r})$, $\mu(\underline{r})$ and $\sigma(\underline{r})$ denote the relative permittivity, the relative permeability, and the conductivity of the scatterers, respectively.

In inverse scattering, the aim is to retrieve the scatterers by defining the distribution of the dielectric properties, $\widehat{\varepsilon}(\underline{r})$, $\widehat{\mu}(\underline{r})$, and $\widehat{\sigma}(\underline{r})$, within Ω starting from a set of (usually noisy) measurements of the electric field $\widetilde{E}_z^{(v)}(\underline{r}_m,t)$ collected a M receivers located at $\underline{r}_m$, $m=1,\ldots,M$.

3 Multi-scaling filtered-FBTS inversion procedure

3.1 Cost function definition

To numerically deal with the inverse scattering problem at hand, the first equation in (2) is discretized according to a *FDTD* scheme [32, 33, 34]. At the s-th step of the *IMSA* procedure ($s=1,\ldots,S$) and p-th iteration of the filtering algorithm ($p=1,\ldots,P$), the region-of-interest (*RoI*) $\Omega^s\big|^p$ ($\Omega^1\big|^p \triangleq \Omega$) is partitioned into N subdomains $\Omega_n^s\big|^p$ centered at $\underline{r}_n^s\big|^p \triangleq \left(x_n^s\big|^p, y_n^s\big|^p\right)$ ($n=1,\ldots,N$, N being the number of degrees of freedom of the scattered field) and the s-th step expansion of the unknowns is considered by defining a set of pulse basis functions $\varphi_n^s(\underline{r})\big|^p = \{1\ if\ \underline{r} \in \Omega_n^s\big|^p; 0\ otherwise\}$

$$\varepsilon^s(\underline{r})\big|^p \triangleq \sum_{n=1}^{N} \varepsilon_n^s\big|^p \varphi_n^s(\underline{r})\big|^p$$

$$\mu^s(\underline{r})\big|^p \triangleq \sum_{n=1}^{N} \mu_n^s\big|^p \varphi_n^s(\underline{r})\big|^p$$

$$\sigma^s(\underline{r})\big|^p \triangleq \sum_{n=1}^{N} \sigma_n^s\big|^p \varphi_n^s(\underline{r})\big|^p.$$

Then, a suitable cost functional is defined [34] to quantify the mismatch between measured and '*estimated*' field data

$$F^s\left(\underline{\varepsilon}^s, \underline{\mu}^s, \underline{\sigma}^s\right)\Big|^p \triangleq \\ \triangleq \int_0^T \left\{ \sum_{v=1}^{V}\sum_{m=1}^{M} \Psi^{(v)}(\underline{r}_m,t)\left|\widetilde{u}^{(v)}(\underline{r}_m,t)\right|^p - u^{(v),s}(\underline{r}_m,t)\Big|^p \right|^2 \Big\} dt \tag{4}$$

where $\underline{\varepsilon}^s\big|^p \triangleq \left[\varepsilon_n^s\big|^p,\ n=1,\ldots,N\right]$, $\underline{\mu}^s\big|^p \triangleq \left[\mu_n^s\big|^p,\ n=1,\ldots,N\right]$, $\underline{\sigma}^s\big|^p \triangleq \left[\sigma_n^s\big|^p,\ n=1,\ldots,N\right]$, $\Psi^{(v)}(\underline{r}_m,t)$ being the v-th weighting function [34] such that

DOI: 10.1587/elex.11.20140578
Received June 16, 2014
Accepted July 14, 2014
Publicized August 1, 2014
Copyedited August 25, 2014

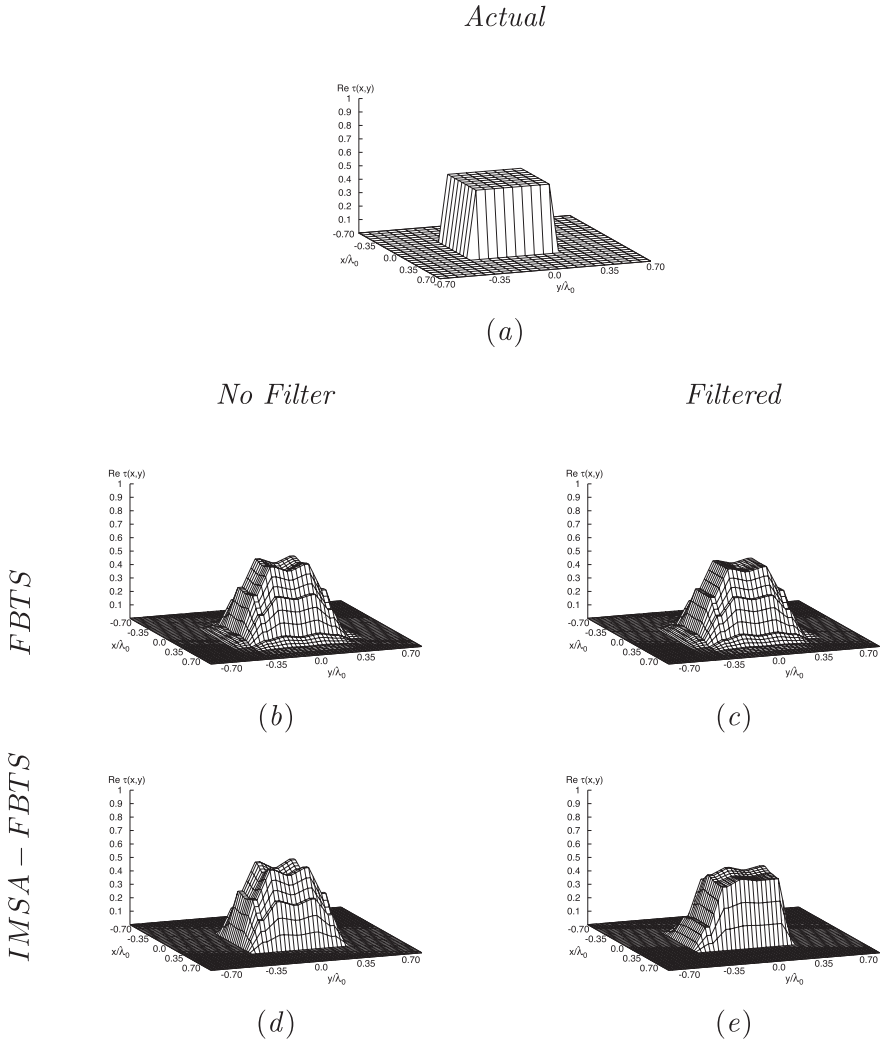

Fig. 2. *Square Centered Cylinder* ($l = 0.8\lambda_0$, $\tau = 0.5$, *Noiseless data*) - Original (a) and retrieved profiles with $(b)(c)$ the FBTS and $(d)(e)$ IMSA-FBTS $(b)(d)$ without and $(c)(e)$ with the filtering.

$\Psi^{(v)}(\underline{r}_m, t = T) = 0$, $\widetilde{u}^{(v)}(\underline{r}, t)$ is the (time-domain) filtered version of the electric field

$$\widetilde{u}^{(v)}(\underline{r}, t)\big|^p \triangleq \int \widetilde{E}_z^{(v)}(\underline{r}, \nu) h(t - \nu)|^p d\tau$$

and $u^{(v),s}(\underline{r}, t)$ is the filtered version of the reconstructed total field at the s-th step of the multiresolution procedure $E_z^{(v),s}(\underline{r}, \tau)$, that is

$$u^{(v),s}(\underline{r}, t)\big|^p \triangleq \int E_z^{(v),s}(\underline{r}, \tau) h(t - \nu)|^p d\tau$$

$h(t)|^p$ being the impulse response of the frequency filter used at the p-th filtering step $(p = 1, \ldots, P)$ [34].

3.2 Iterative minimization process

Thanks to the choice of a number of unknowns close to the number of measured data samples, numerically efficient local search approaches can be considered to minimize (4) because of the reduced occurrence of local minima

DOI: 10.1587/elex.11.20140578
Received June 16, 2014
Accepted July 14, 2014
Publicized August 1, 2014
Copyedited August 25, 2014

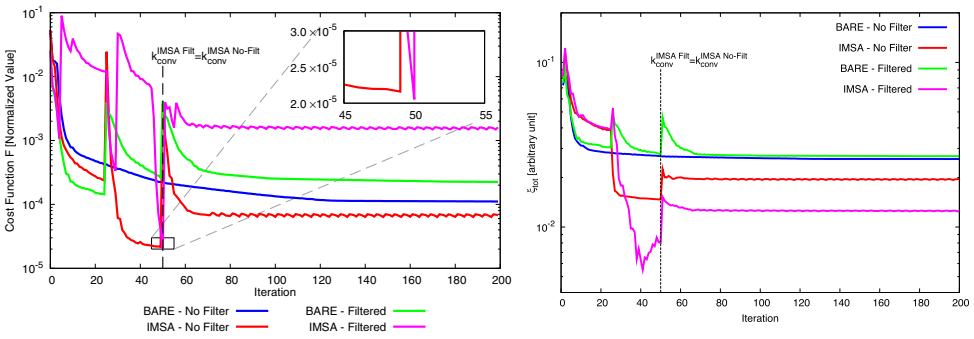

Fig. 3. *Square Centered Cylinder* ($l = 0.8\lambda_0$, $\tau = 0.5$, *Noiseless data*) - Plots of (a) the cost function and (b) the total reconstruction error vs. the iteration number.

[45]. Accordingly, a gradient-based technique is used. For the sake of conciseness, let us detail the procedure for the inversion of the dielectric profile since very similar guidelines and expressions can be derived for the unknown permeability and conductivity, as well. Towards this end, starting from an initial ($k = 0$) guess solution[1] $\underline{\varepsilon}^s\big|_0^p$, the s-th step trial solution $\underline{\varepsilon}^s$ is iteratively computed

$$\underline{\varepsilon}^s\big|_{k+1}^p = \underline{\varepsilon}^s\big|_k^p + \alpha^s\big|_k^p \underline{d}^s\big|_k^p \quad k = 1, \ldots, K \tag{5}$$

where K is the total number of iterations of the gradient-based iterative procedure (k being the iteration number), $\alpha^s\big|_k^p$ is the *step-size* and $\underline{d}^s\big|_k^p$ the *search direction* determined according to the Polak-Ribiere approach [33, 34]

$$\underline{d}^s\big|_{k+1}^p = -\underline{g}^s\big|_{k+1}^p + \frac{\left\langle \underline{g}^s\big|_{k+1}^p - \underline{g}^s\big|_k, \underline{g}^s\big|_{k+1}^p \right\rangle}{\left\langle \underline{g}^s\big|_k^p, \underline{g}^s\big|_k^p \right\rangle} \underline{d}^s\big|_k^p. \tag{6}$$

$\langle \cdot, \cdot \rangle$ being the inner product symbol. Moreover, $\underline{g}^s\big|_k^p \triangleq \left\{ g_n^s\big|_k^p,\ n = 1, \ldots, N \right\}$ is the gradient of $\underline{F}^s\left(\underline{\varepsilon}^s, \underline{\mu}^s, \underline{\sigma}^s\right)\big|^p$ with respect to the unknown dielectric distribution at the k-th step [34] whose explicit expression is derived by applying the Riesz representation theorem [33]

$$g_n^s\big|_k^p = 2 \int_{\Omega_n^s\big|^p} \left\{ \int_0^T \left[\sum_{v=1}^{V} \left(w_1^{(v),s}(\underline{r}, t)\big|_k^p \frac{\partial u^{(v),s}(\underline{r}, t)}{\partial (ct)} \right) \right] dt \right\} d\underline{r}$$

where $E_z^{(v),s}(\underline{r}, t)\big|_k$ is the E-field related to the v-th source and due to the estimated scatterer distribution at the k-th gradient step of the s-th *IMSA* iteration, while $w_1^{(v),s}(\underline{r}, t)\big|_k^p$ is the so-called *adjoint field* computed by solving the following *adjoint problem* [33]

$$\mathcal{L}^\star \begin{bmatrix} w_1^{(v),s}(\underline{r}, t)\big|_k^p \\ w_2^{(v),s}(\underline{r}, t)\big|_k^p \\ w_3^{(v),s}(\underline{r}, t)\big|_k^p \end{bmatrix} = \begin{bmatrix} \sum_{m=1}^{M} \delta(\underline{r} - \underline{r}_m) \Psi^{(v)}(\underline{r}_m, t) \times \\ \times \left[\widetilde{u}^{(v)}(\underline{r}, t)\big|^p - u^{(v),s}(\underline{r}_m, t)\big|^p \right] \\ 0 \\ 0 \end{bmatrix} \tag{7}$$

[1] $\underline{\varepsilon}^1\big|_0^1$ is set to the free space distribution.

DOI: 10.1587/elex.11.20140578
Received June 16, 2014
Accepted July 14, 2014
Publicized August 1, 2014
Copyedited August 25, 2014

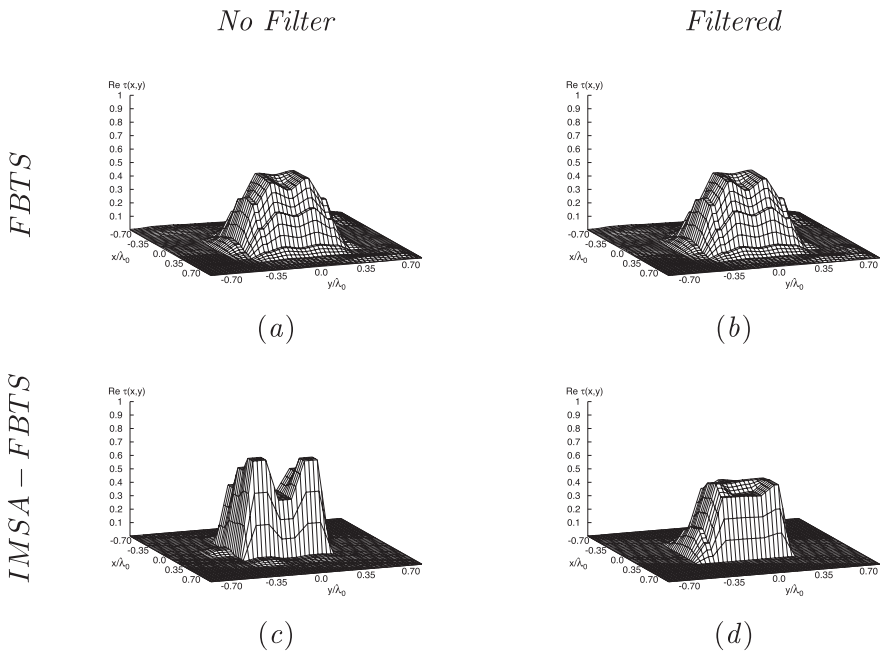

Fig. 4. *Square centered cylinder* ($l = 0.8\lambda_0$, $\tau = 0.5$, $SNR = 10\,\mathrm{dB}$) - Retrieved profiles with $(a)(b)$ the $FBTS$ and $(c)(d)$ the $IMSA - FBTS$ $(a)(c)$ without and $(b)(d)$ with the filtering.

under the initial condition $w_1^{(v),s}(\underline{r}, t = T)\big|_k^p = w_2^{(v),s}(\underline{r}, t = T)\big|_k^p = w_3^{(v),s}(\underline{r}, t = T)\big|_k^p = \underline{0}$, $\mathcal{L}^\star$ being the adjoint field operator [33]

$$\mathcal{L}^\star = \frac{\partial}{\partial x}\mathbf{A}' - \frac{\partial}{\partial y}\mathbf{B}' - \frac{\partial}{\partial (ct)}\mathbf{C}' - \mathbf{D}'. \tag{8}$$

To numerically implement (5), the step size $\alpha^s\big|_k^p$ in (5) is straightforwardly determined through a line search strategy (see [33] for details).

3.3 Termination condition

Once the s-th *IMSA* step has been completed by applying (5) for K iterations, a suitable zooming procedure is performed ($s \leftarrow s+1$) to update the *RoI* ($\Omega^s\big|^p \leftarrow \Omega^{s+1}\big|^p$) where selectively increasing the spatial resolution of the inversion [39]. More specifically, the *acquired information* at the s-th step is used to compute the center $\underline{r}^{s+1}\big|^p \triangleq \left(x^{s+1}\big|^p, y^{s+1}\big|^p\right)$ of the updated *RoI* as follows [39]

$$\begin{cases} x^{s+1}\big|^p \triangleq \dfrac{\sum_{n=1}^N x_n^s\big|^p \varepsilon_n^s\big|^p}{\sum_{n=1}^N \varepsilon_n^s\big|^p} \\ y^{s+1}\big|^p \triangleq \dfrac{\sum_{n=1}^N y_n^s\big|^p \varepsilon_n^s\big|^p}{\sum_{n=1}^N \varepsilon_n^s\big|^p} \end{cases}$$

as well as its size as detailed in [39]. The reconstruction process is then repeated until suitable *IMSA* termination conditions [39] are satisfied ($s = S$) and the corresponding dielectric distribution, $\underline{\varepsilon}^S\big|^p$, is assumed as the retrieved solution at the p-th filtering step to be employed for the successive filtering ($p \leftarrow p+1$) for re-initializing Eq. (5) as follows

DOI: 10.1587/elex.11.20140578
Received June 16, 2014
Accepted July 14, 2014
Publicized August 1, 2014
Copyedited August 25, 2014

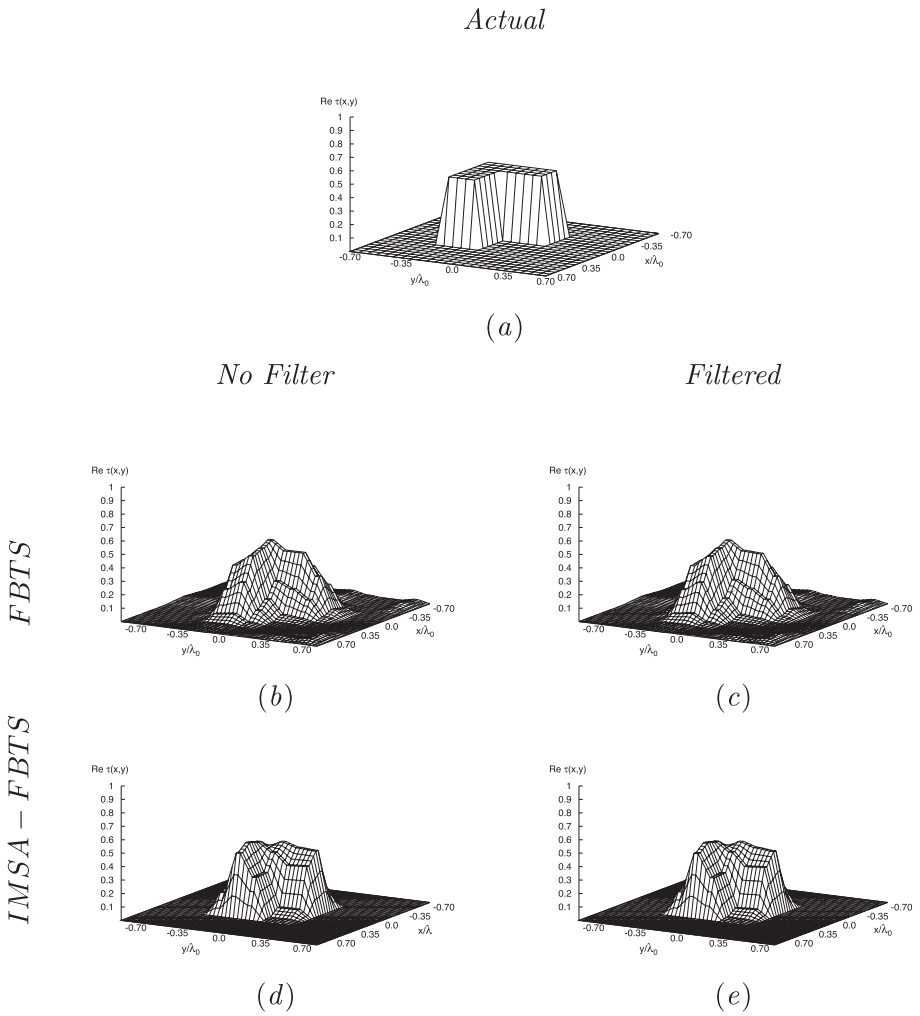

Fig. 5. *L-Shaped Cylinder* ($\tau = 0.5$, $SNR = 10\,\mathrm{dB}$) - Original (a) and retrieved profiles with $(b)(c)$ the $FBTS$ and $(d)(e)$ the $IMSA - FBTS$ $(b)(d)$ without and $(c)(e)$ with filtering.

$$\underline{\varepsilon}^s\big|_0^{p+1} \triangleq \underline{\varepsilon}^S\big|^p \tag{9}$$

by defining a $h(t)|^{p+1}$ with a higher cut-off frequency [34].

The overall process is then stopped when one of the following termination conditions holds true

C. 1 P filtering steps are carried out [34], P being a used-defined parameter;

C. 2 The cost function $F^s\left(\underline{\varepsilon}^s, \underline{\mu}^s, \underline{\sigma}^s\right)\big|^p$ stagnates or starts increasing between two successive $IMSA$ iterations;

C. 3 The zooming process stagnates (i.e., $\Omega^s|^p \approx \Omega^{s+1}\big|^p$).

4 Numerical results

This section is aimed at illustrating the key-features of the multi-resolution filtered forward-backward time-stepping method ($IMSA - FBTS$) as well as numerically assessing potentialities and limitations of the proposed approach when dealing with noiseless and noisy data. Towards this end, let us consider a set of lossless non-magnetic scatterers $[\sigma(\underline{r}) = 0.0,\ \mu(\underline{r}) = 1.0]$ lying within

DOI: 10.1587/elex.11.20140578
Received June 16, 2014
Accepted July 14, 2014
Publicized August 1, 2014
Copyedited August 25, 2014

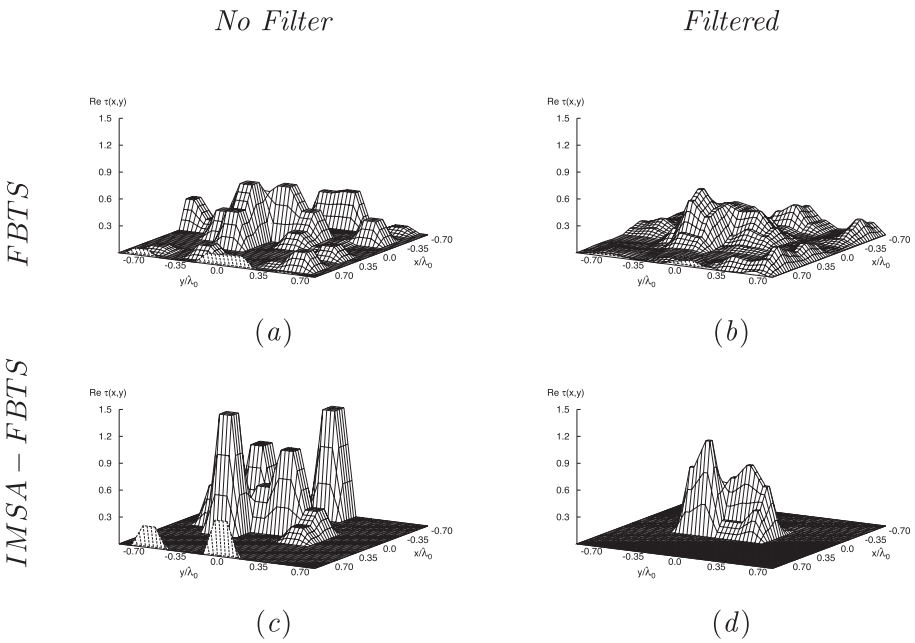

Fig. 6. *L-Shaped Cylinder* ($\tau = 0.5$, $SNR = -10\,\mathrm{dB}$) - Retrieved profiles with $(a)(b)$ the *FBTS* and $(c)(d)$ the $IMSA - FBTS$ $(a)(c)$ without and $(b)(d)$ with filtering.

an investigation domain Ω of side $\ell = 0.25 \times 10^{-1}$ [m]. As for the scattering data, $M = 16$ equally-spaced measurement points have been located on a circle of radius $\rho = 0.25$ [m] [Fig. 1(a)] as the $V = 16$ illumination sources radiating Gaussian pulses with pulse-shape [Fig. 1(b)]

$$I(t) \triangleq \exp\left(-\frac{t - 100\Delta t}{\Gamma}\right)^2 sin\left[\frac{2\pi c}{\lambda_0}(t - 100\Delta t)\right]$$

$\lambda_0 = 0.15\,\mathrm{m}$ being the *central wavelength* and $\Gamma = 2.8826 \times 10^{-10}$ [s].

As far as the inversion is concerned, an *IMSA* grid of $N = 5 \times 5$ square sub-domains has been used to partition the *RoI*, while the following parameter setup has been heuristically chosen: $K = 200$, $S = 4$, $P = 3$. Moreover, the *FDTD* scheme has been applied with $\Delta t = 23.041 \times 10^{-12}$ [s], $\Delta x = \Delta y = 2.55 \times 10^{-3}$ [m], and employing *PML* boundary conditions [33]. Concerning the filtering process, a 4-th order low-pass Chebyshev filter with p-th $(p = 1, \ldots, P)$ cutoff frequency $\chi_0|^p$ has been assumed [34]

$$h(t)|^p \triangleq \int_{-\infty}^{\infty} \Phi(\chi)|^p \exp(2\pi i t\chi) d\chi$$

where

$$\Phi(\chi)|^p \triangleq \frac{\gamma_1\gamma_2(\chi_0|^p)^4(1+e^2)^{-1/2}}{\prod_{q=1}^{2}\left[\chi^2 - i2\kappa_q\chi\,\chi_0|^p - \gamma_q(\chi_0|^p)^2\right]}$$

and $e = 0.15$, $\kappa_1 = 0.2661$, $\kappa_2 = 0.6425$, $\gamma_1 = 13372$, $\gamma_2 = 0.6301$. More specifically, $\chi_0|^p$ has been selected so that

DOI: 10.1587/elex.11.20140578
Received June 16, 2014
Accepted July 14, 2014
Publicized August 1, 2014
Copyedited August 25, 2014

$$\beta|^p = \frac{\sum_{v=1}^{V}\sum_{m=1}^{M}\int_0^T\left[\widetilde{u}^{(v)}(\underline{r},t)\right|^p\Big]^2 dt}{\sum_{v=1}^{V}\sum_{m=1}^{M}\int_0^T\left[\widetilde{E}_z^{(v)}(\underline{r}_m,t)\right]^2 dt} \tag{10}$$

$\beta|^1 = 0.01$ (i.e., $\chi_0|^1 = 1.43\,\mathrm{GHz}$), $\beta|^2 = 0.50$ (i.e., $\chi_0|^2 = 2.24\,\mathrm{GHz}$), and $\beta|^3 = 0.99$ (i.e., $\chi_0|^3 = 3.10\,\mathrm{GHz}$).

The first numerical example deals with the reconstruction of a square centered cylinder [Fig. 2(a)] with side $l = 0.8\lambda_0$ and contrast $\tau(\underline{r}) = 0.5$ ($\tau(\underline{r}) \triangleq \varepsilon(\underline{r}) - 1$ [39]). By comparing the performances of the proposed filtered $IMSA - FBTS$ approach [Fig. 2(e)] with that obtained by the filtered $FBTS$ technique [34] [Fig. 2(c)], it turns out that the multi-resolution procedure enhances in a non-negligible way the retrieval accuracy. Similar outcomes arise also neglecting the filtering process [Fig. 2(b) vs. Fig. 2(d)]. Such a result actually indicates that, on the one hand, the $IMSA$ procedure improves the $FBTS$ effectiveness [e.g., Fig. 2(e) vs. Fig. 2(c)] and, on the other hand, such a filtering does not cut-off relevant information from the data [e.g., Fig. 2(d) vs. Fig. 2(e)].

As for the minimization of the cost function, Fig. 3(a) shows its iterative evolution when *Conditions 2* and *3* have been neglected. The multi-resolution process matches the measured data more carefully than the standard $FBTS$ implementation as indicated by the lower cost function values at the termination [Fig. 3(a)]. Moreover, the plots of the integral error ξ [39]

$$\xi_{tot} = \frac{\int_\Omega |[\varepsilon(\underline{r}) - \widehat{\varepsilon}(\underline{r})]| d\underline{r}}{\int_\Omega \varepsilon(\underline{r}) d\underline{r}} \tag{11}$$

show that smaller cost function values actually correspond to more accurate reconstructions [Fig. 3(b)]. This suggests/confirms that a stopping criterion based on a convergence threshold on the cost function value (i.e., *Condition 2*) provides a reliable tool for guaranteeing the inversion results in practical cases when ξ_{tot} cannot be evaluated.

To investigate whether previous deductions also extend to noisy conditions, the same retrieval problem has been solved when adding the scattering data with a Gaussian noise $\Xi^{(v)}(\underline{r}_m,t)$ with a signal-to-noise ratio (SNR) before the *filtering* [34] equal to $SNR = 10\,\mathrm{dB}$ being

$$SNR \triangleq 10\log_{10}\frac{\sum_{v=1}^{V}\sum_{m=1}^{M}\int_0^T\left|\widetilde{E}_z^{(v)}(\underline{r}_m,t)\right|^2 dt}{\sum_{v=1}^{V}\sum_{m=1}^{M}\int_0^T|\Xi^{(v)}(\underline{r}_m,t)|^2 dt}. \tag{12}$$

The estimated profiles (Fig. 4) further confirm that the $IMSA$-based implementation yields better reconstructions especially in the filtered case [Fig. 4(d) vs. Fig. 4(b)]. Unlike the noiseless scenario, the filtering has here a non-negligible impact on the inversion despite the high level of noise [e.g., Fig. 4(d) vs. Fig. 4(c)].

Similar conclusions can be drawn when more complicated profiles are at hand. Fig. 5 refers to a L-shaped scatterer [Fig. 5(a)] when $SNR = 10\,\mathrm{dB}$, while heavier conditions are analyzed in Fig. 6 ($SNR = -10\,\mathrm{dB}$). Although already evident in the former case (Fig. 5), this latter test clearly assesses a significantly improved accuracy of the filtered $IMSA - FBTS$ approach

DOI: 10.1587/elex.11.20140578
Received June 16, 2014
Accepted July 14, 2014
Publicized August 1, 2014
Copyedited August 25, 2014

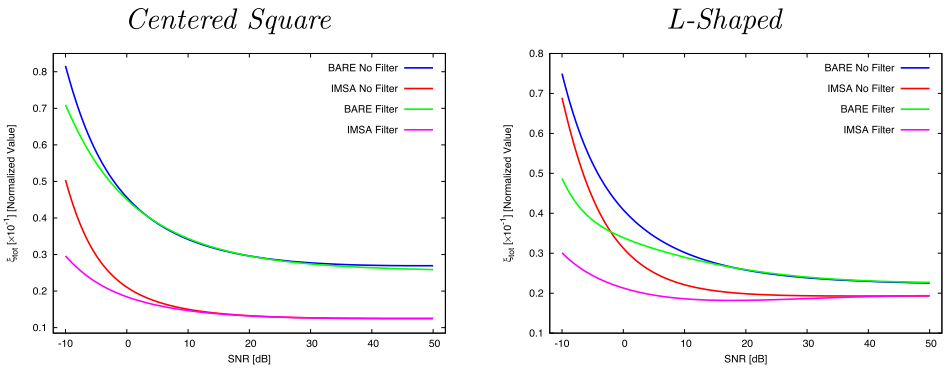

Fig. 7. Total reconstruction error vs. *SNR* when reconstructing (a) the "Centered Square" and (b) the "L-Shaped" profiles.

[Fig. 6(d)] compared to both the standard *FBTS*-filtered [Fig. 6(b)] and the non-filtered *IMSA* − *FBTS* [Fig. 6(c)] implementations, then confirming the usefulness of integrating the filtering and the multi-focusing procedures.

The last result is devoted to give an overview of the method performance when varying the *SNR* level. Towards this end, the behaviour of the integral error as a function of the *SNR* for both dielectric profiles is analyzed in Fig. 7. As it can be observed (a) the *IMSA* strategy allows one to enhance the reconstruction accuracy with respect to the standard *FBTS* implementation [Fig. 7(a)]; (b) whatever the implementation and for low noise conditions, the filtering does not sensibly affect the reconstruction [Fig. 7(b)]; (c) the filtered *IMSA* − *FBTS* yields to more faithful reconstructions when the *SNR* reduces [Fig. 7(b)].

5 Conclusions

To effectively address the *ill-posedness* and the *non-linearity* of time-domain electromagnetic inversions, an innovative microwave imaging approach has been presented. It combines the regularization capabilities of the filtered *FBTS* method with the information-acquisition features of the *IMSA*. A set of representative numerical results have been discussed to assess features, potentialities, and robustness of the proposed implementation. The numerical analysis even though preliminary has proved that (i) the *IMSA* enhances the accuracy and robustness of the *FBTS* time-domain filtered as well as non-filtered data inversions (Fig. 7); (ii) the filtering does not degrade the reconstruction when noiseless or low-noise data are at hand (Fig. 2), while it significantly enhances the method robustness against noisy data (Fig. 6); (iii) whatever the scatterer and the scenario at hand, the filtered *IMSA* − *FBTS* technique overcomes previous state-of-the-art *FBTS*-based approaches.

Acknowledgments

This work was supported in part by a Grant-in-Aid for Scientific Research (C) Number 25420411.

DOI: 10.1587/elex.11.20140578
Received June 16, 2014
Accepted July 14, 2014
Publicized August 1, 2014
Copyedited August 25, 2014